Superconductivity in a model of two Hubbard chains coupled with ferromagnetic exchange interaction

T. Shirakawa
Graduate School of Science and Technology, Chiba University, Chiba 263-8522, Japan

S. Nishimoto
Leibniz-Institut für Festkörper- und Werkstoffforschung Dresden, P.O. Box 270116, 01171 Dresden, Germany

Y. Ohta
Department of Physics, Chiba University, Chiba 263-8522, Japan
(Dated: March 18, 2008)

We study the ground-state properties of the double-chain Hubbard model coupled with ferromagnetic exchange interaction by using the weak-coupling theory, density-matrix renormalization group technique, and Lanczos exact-diagonalization method. We determine the ground-state phase diagram in the parameter space of the ferromagnetic exchange interaction and band filling. We find that, in high electron density regime, the spin gap opens and the spin-singlet d_{xy}-wave-like pairing correlation is most dominant, whereas in low electron density regime, the fully-polarized ferromagnetic state is stabilized where the spin-triplet p_y-wave-like pairing correlation is most dominant.

PACS numbers: 71.10.Fd, 71.10.Hf, 74.20.Mn, 74.20.Rp

arXiv:0803.2590v1 [cond-mat.str-el] 18 Mar 2008

I. INTRODUCTION

Ferromagnetism in itinerant electron systems has increasingly been understood since the Hubbard model was introduced in 1963.[1,2] It is known that subtle interplay between quantum many-body effects and spin-independent Coulomb interactions plays a crucial role in generating ferromagnetic orders in some solids;[3] a variety of origins such as Nagaoka-Thouless mechanism,[4,5] flat-band,[6,7] orbital degeneracy,[8,9,10] three-site ring exchange interaction,[11,12] etc., have so far been proposed. In addition to ferromagnetism, (possibly) spin-triplet superconductivity was recently discovered in the metallic ferromagnets UGe_2,[13] URhGe,[14] and $ZrZn_2$.[15] Consequently, the relation between superconductivity and ferromagnetism has been of special interest in the field of strongly correlated systems. From the theoretical point of view, the occurrence of superconductivity in ferromagnetic materials is naturally explained by the formation of Cooper pairs with parallel spins, namely, spin-triplet pairs.[16]

Among the origins of ferromagnetism mentioned above, only the three-site ring exchange interaction acts on a couple of electrons. It yields a ferromagnetic spin correlation, which in turn produces an attractive effect between them. One may easily imagine that a spin-triplet superconductivity is realized if the attractive interaction between electrons can survive against the other effects. Recently, we have confirmed that this mechanism actually works in a fairly simple correlated electron system; the system consists of two Hubbard chains coupled with zigzag bonds and has a unique structure of hopping integrals.[17,18,19] In this model, the spin-triplet pairing of electrons occurs between the inter-chain neighboring sites. If the ferromagnetic correlation between the two chains are essential for the spin-triplet superconductivity, we may be allowed to mimic our original model by a double-chain Hubbard model coupled with ferromagnetic exchange interaction. This new model is much easier to analyze than the original one due to the reduction of quantum fluctuations. Therefore, the introduction of this model will enable us to investigate the spin-triplet superconductivity in more detail for wide range of parameters.

In this paper, we thus study the double-chain Hubbard model coupled with ferromagnetic exchange interaction. We use the weak-coupling bosonization/renormalization group (RG) analyses,[20] the density-matrix renormalization group (DMRG) technique, and the Lanczos exact-diagonalization method.[22] We thereby determine the ground-state phase diagram: we find that, in the high electron density regions, the spin gap opens and the d_xy-wave-like pairing occurs, while in the low electron density regions, the system is in the metallic state with full spin polarization, where the p_y-wave-like spin-triplet pairing correlation becomes the most dominant. We note that this model can be regarded as a single-chain model with two degenerate orbitals if we assume the ferromagnetic exchange interaction to be identified with the intra-atomic Hund's rule coupling. This single-chain model has so far been studied both analytically[23,24,25] and numerically[26,27]. It has been proposed that the Haldane gap state is realized at half filling. It has also been pointed out that the system remains gapful for low hole doping regions.[28]

Our paper is organized as follows. In Sec. II, we define the double-chain Hubbard model coupled with ferromagnetic exchange interaction. In Sec. III, we analyze the model using the weak-coupling theory and derive the pairing order parameter. In Sec. IV, we calculate several quantities with the DMRG and Lanczos methods and present the calculated results. We also check if the results

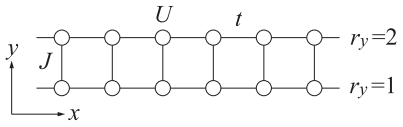

FIG. 1: Schematic representation of the double-chain Hubbard model coupled with ferromagnetic exchange interaction. No hopping process is allowed between the two chains and no exchange interactions exist along the chains.

are consistent with the weak-coupling results. Section V contains summary and conclusions.

II. MODEL

We study the double-chain Hubbard model coupled with ferromagnetic exchange interaction (see Fig. 1), the Hamiltonian of which is defined by

$$\begin{aligned} H = \; & t \sum_{r_x,r_y,\sigma} \left(c^\dagger_{r_x,r_y,\sigma} c_{r_x+1,r_y,\sigma} + \text{H.c.} \right) \\ & + U \sum_{r_x,r_y} n_{r_x,r_y,\uparrow} n_{r_x,r_y,\downarrow} \\ & - J \sum_{r_x} \mathbf{S}_{r_x,1} \cdot \mathbf{S}_{r_x,2} \end{aligned} \tag{1}$$

where $c^\dagger_{r_x,r_y,\sigma}$ ($c_{r_x,r_y,\sigma}$) is the creation (annihilation) operator of an electron with spin σ ($=\uparrow,\downarrow$) at site r_x on leg r_y ($=1,2$), $n_{r_x,r_y,\sigma} = c^\dagger_{r_x,r_y,\sigma} c_{r_x,r_y,\sigma}$ is the density operator, and $\mathbf{S}_{r_x,r_y}$ is the spin-$\frac{1}{2}$ operator. t is the nearest-neighbor hopping integral along the chain, U is the onsite Coulomb interaction, and $J(>0)$ is the ferromagnetic exchange interaction between two sites on each rung. Note that no hopping process is allowed between the two chains and thus the two bands are degenerate.

III. WEAK-COUPLING THEORY

We first consider the weak-coupling regime where only the low-energy excitations near the Fermi points are crucial. Thus far, the weak-coupling theory has been well-constructed for two-band models.[24,30,31,32,33,34,35,36,37] We further develop the approach to analyze the Hamiltonian (1). Assuming a linearization of the dispersion relations in the vicinity of the Fermi level, we introduce the field operators of right- and left-going electrons as

$$\psi_{p,\sigma,\pm}(x) = \frac{1}{\sqrt{L}} \sum_{k_x} e^{ikx} c^\pm_{p,\sigma}(k) \tag{2}$$

where $c^\pm_{p,\sigma}$ is the Fourier transform of combined operator $(c_{r_x,1,\sigma} \pm c_{r_x,1,\sigma})/\sqrt{2}$ for the right-going ($p=+$) and left-going ($p=-$) electrons. L is the chain length where the lattice spacing is set to be unity. Using these field operators, the Hamiltonian can be rewritten as a sum of the linearized kinetic energy and interaction terms. We thus obtain

$$\begin{aligned} H = \; & \int dx H_0 + \int dx H_I \\ H_0 = \; & v_{\rm F} \sum_{p,\sigma,\zeta} \psi^\dagger_{p,\sigma,\zeta} \left(-ip \frac{d}{dx} \right) \psi_{p,\sigma,\zeta} \\ H_I = \; & \frac{1}{4} \sum_{p,\sigma} \sum_{\zeta} {}' g^{\epsilon,\bar\epsilon}_{1\perp} \psi^\dagger_{p,\sigma,\zeta_1} \psi^\dagger_{-p,-\sigma,\zeta_2} \psi_{p,-\sigma,\zeta_4} \psi_{-p,\sigma,\zeta_3} \\ & \frac{1}{4} \sum_{p,\sigma} \sum_{\zeta} {}' g^{\epsilon,\bar\epsilon}_{2\perp} \psi^\dagger_{p,\sigma,\zeta_1} \psi^\dagger_{-p,-\sigma,\zeta_2} \psi_{-p,-\sigma,\zeta_4} \psi_{p,\sigma,\zeta_3} \\ & \frac{1}{4} \sum_{p,\sigma} \sum_{\zeta} {}' g^{\epsilon,\bar\epsilon}_{\parallel} \psi^\dagger_{p,\sigma,\zeta_1} \psi^\dagger_{-p,\sigma,\zeta_2} \psi_{p,\sigma,\zeta_4} \psi_{-p,\sigma,\zeta_3}. \end{aligned} \tag{3}$$

where $\epsilon = \zeta_1\zeta_3$ and $\bar\epsilon = \zeta_1\zeta_2$. The primed summation over $\zeta_i (i = 1,2,3,4)$ is restricted by a relation $\zeta_1\zeta_2\zeta_3\zeta_4 = +1$, which comes from the momentum conservation condition in the transverse components. The coupling constants $g^{\epsilon,\bar\epsilon}_{1\perp}$ and $g^{\epsilon,\bar\epsilon}_{2\perp}$ are related to the original parameters in the Hamiltonian (1):

$$\begin{aligned} & g^{++}_{1\perp} = U, \quad g^{+-}_{1\perp} = -\frac{J}{4}, \quad g^{--}_{1\perp} = -\frac{J}{2}, \\ & g^{++}_{2\perp} = U, \quad g^{+-}_{2\perp} = -\frac{J}{4}, \quad g^{--}_{2\perp} = -\frac{J}{2}. \end{aligned} \tag{4}$$

For the SU(2) symmetric case, we can choose

$$g^{++}_{\parallel} = g^{++}_{1\perp} - g^{++}_{2\perp} \tag{5}$$

$$g^{-+}_{\parallel} = g^{-+}_{1\perp} - g^{-+}_{2\perp} \tag{6}$$

$$g^{+-}_{\parallel} = g^{+-}_{1\perp} - g^{--}_{2\perp} \tag{7}$$

$$g^{--}_{\parallel} = g^{--}_{1\perp} - g^{+-}_{2\perp}. \tag{8}$$

In this Section III, we consider the case away from half filling. Hence, the Umklapp term g_3 gives no contribution and the Fermi velocity renormalization due to the forward-scattering term g_4 may be neglected.

A. Bosonization

Using the Abelian bosonization method,[29] we introduce eight chiral bosonic fields $\phi^p_{\mu r}$ where μ refers to the charge (ρ) and spin (σ) sectors; meanwhile, r refers to the even ($+$) and odd ($-$) sectors. The bosonic fields satisfy the commutation relations $[\phi^\pm_{\mu r}(x), \phi^\pm_{\mu' r'}(x')] = \pm i(\pi/4)\text{sgn}(x-x')\delta_{\mu,\mu'}\delta_{r,r'}$ and $[\phi^+_{\mu r}(x), \phi^-_{\mu' r'}(x')] = i(\pi/4)\delta_{\mu,\mu'}\delta_{r,r'}$. We then define a new set of chiral bosonic fields as

$$\phi_{p,s,\zeta} = \phi^p_{\rho+} + \zeta\phi^p_{\rho-} + s\phi^p_{\sigma+} + s\zeta\phi^p_{\sigma-} \tag{9}$$

where $p=\pm$, $s=\pm$, and $\zeta=\pm$. The chiral bosons obey the commutation relations $[phi_{p,s,\zeta}(x), phi_{p,s',\zeta'}(x')] =$

$\pm i(\pi/4)\mathrm{sgn}(x-x')\delta_{p,p'}\delta_{s,s'}$ and $[\phi_{+,s,\zeta}(x),\phi_{-,s',\zeta'}(x')] = i(\pi/4)\delta_{s,s'}\delta_{\zeta,\zeta'}$. The field operators of the right-moving and left-moving electrons (2) are then written as

$$\psi_{p,\sigma,\zeta} = \frac{\eta_{\sigma,\zeta}}{\sqrt{2\pi a}} \exp\left(ipk_{\mathrm{F}}x + ip\phi_{p,s,\zeta}\right) \tag{10}$$

where $s = +(-)$ for $\sigma =\uparrow (\downarrow)$. The Majorana fermions $\eta_{\sigma,\zeta}$, known as Klein factors, are introduced to ensure the proper anticommutation relations between fermion fields with different band and spin indices. They obey $\{\eta_{\sigma,\zeta},\eta_{\sigma',\zeta'}\} = 2\delta_{\sigma,\sigma'}\delta_{\zeta,\zeta'}$. It is generally more convenient to trade the chiral boson fields pairwise for a conventional bosonic phase field ϕ and its dual field θ, so that we also introduce the bosonic fields given by

$$\phi_{\mu,r} = \phi^{+}_{\mu,r} + \phi^{-}_{\mu,r} \tag{11}$$

$$\theta_{\mu,r} = \phi^{+}_{\mu,r} - \phi^{-}_{\mu,r}, \tag{12}$$

where the operator $\Pi_{\mu r}(x) = \partial_x\theta_{\mu r}/\pi$ is a canonical conjugate variable to $\phi_{\mu r}$, which satisfies $[\phi_{\mu r}(x),\Pi_{\mu r}(x')] = i\delta(x-x')\delta_{\mu,\mu'}\delta_{r,r'}$.

Now, we can rewrite the noninteracting term of the Hamiltonian (3) as

$$H_0 = \frac{v_{\mathrm{F}}}{2\pi}\sum_{\mu=\rho,\sigma}\sum_{r=\pm}\left[\left(\partial_x\theta_{\mu,r}\right)^2 + \left(\partial_x\phi_{\mu,r}\right)^2\right]. \tag{13}$$

On the other hand, the interacting term is more complicated, containing many products of the Klein factors such as $\hat{\Gamma} \equiv \eta_{\uparrow,+}\eta_{\downarrow,+}\eta_{\uparrow,-}\eta_{\uparrow,-}$, $\hat{h_\sigma} \equiv \eta_{\sigma,+}\eta_{\sigma,-}$, and $\hat{h_\zeta}' \equiv \eta_{\uparrow,\zeta}\eta_{\downarrow,\zeta}$. However, it is known that their eigenvalues are $\Gamma = \pm 1$, $h_\sigma = \pm i$, and $h'_\zeta = \pm i$.[37] Thus, if we adopt the following convention $\Gamma = +1$, $h_\sigma = i$, $h'_\zeta = i\zeta$, the interacting term is reduced to

$$\begin{aligned} H_I \quad = & \sum_{\mu=\rho,\sigma}\sum_{r=\pm}\frac{g_{\mu,r}}{2\pi^2}\partial_x\phi^{+}_{\mu,r}\partial_x\phi^{-}_{\mu,r} + \\ & \frac{1}{2\pi^2}\left[\left(g^{+-}_{1\perp} - g^{--}_{2\perp}\right)\cos 2\phi_{\rho-}\cos 2\phi_{\sigma-}\right. \\ & + \left(g^{-+}_{1\perp} - g^{-+}_{2\perp}\right)\cos 2\theta_{\rho-}\cos 2\theta_{\sigma-} \\ & + g^{++}_{1\perp}\cos 2\phi_{\sigma+}\cos 2\phi_{\sigma-} + g^{+-}_{1\perp}\cos 2\phi_{\rho-}\cos 2\phi_{\sigma+} \\ & - g^{-+}_{1\perp}\cos 2\theta_{\rho-}\cos 2\phi_{\sigma+} + g^{--}_{1\perp}\cos 2\phi_{\sigma+}\cos 2\theta_{\sigma-} \\ & \left. - g^{-+}_{2\perp}\cos 2\theta_{\rho-}\cos 2\phi_{\sigma-} + g^{--}_{2\perp}\cos 2\phi_{\rho-}\cos 2\theta_{\sigma-}\right] \end{aligned} \tag{14}$$

with

$$g_{\rho+} = -g^{++}_{1\perp} + 2g^{++}_{2\perp} - g^{--}_{1\perp} + g^{+-}_{2\perp} \tag{15}$$

$$g_{\rho-} = -g^{++}_{1\perp} + 2g^{++}_{2\perp} + g^{--}_{1\perp} - g^{+-}_{2\perp} \tag{16}$$

$$g_{\sigma+} = -g^{++}_{1\perp} - 2g^{--}_{1\perp} \tag{17}$$

$$g_{\sigma-} = -g^{++}_{1\perp} + 2g^{--}_{1\perp}. \tag{18}$$

If we use the notation with $g_{\mu,r}$, H_0 can also be written as

$$H'_0 = \sum_{\mu,r}\frac{u_{\mu,r}}{2\pi}\left[K_{\mu,r}\left(\partial_x\theta_{\mu,r}\right)^2 + K^{-1}_{\mu,r}\left(\partial_x\phi_{\mu,r}\right)^2\right] \tag{19}$$

with the critical exponents

$$K_{\mu,r} = \sqrt{\frac{2\pi v_{\mathrm{F}} - g_{\mu,r}}{2\pi v_{\mathrm{F}} + g_{\mu,r}}} \tag{20}$$

and the renormalized Fermi velocity

$$u_{\mu,r} = v_{\mathrm{F}}\sqrt{1 - \left(\frac{g_{\mu,r}}{2\pi v_{\mathrm{F}}}\right)^2}. \tag{21}$$

B. Renormalization-group analysis

By treating the interaction perturbatively, we derive the renormalization group (RG) equations in the one-loop level as follows:

$$\begin{aligned} \frac{\partial g^{++}_{1\perp}}{\partial S} \;=\; & -2\left(g^{++}_{1\perp}\right)^2 - 2g^{-+}_{1\perp}g^{-+}_{2\perp} \\ & -2\left(g^{+-}_{1\perp}\right)^2 + 2g^{+-}_{1\perp}g^{--}_{2\perp} \end{aligned} \tag{22}$$

$$\begin{aligned} \frac{\partial g^{-+}_{1\perp}}{\partial S} \;=\; & -2g^{-+}_{1\perp}g^{++}_{2\perp} - 2g^{-+}_{2\perp}g^{++}_{1\perp} - 4g^{-+}_{1\perp}g^{--}_{1\perp} \\ & +2\left(g^{-+}_{1\perp}g^{+-}_{2\perp} + g^{--}_{1\perp}g^{-+}_{2\perp}\right) \end{aligned} \tag{23}$$

$$\begin{aligned} \frac{\partial g^{1\perp}_{--}}{\partial S} \;=\; & -2\left(g^{-+}_{1\perp}\right)^2 - 2\left(g^{--}_{1\perp}\right)^2 \\ & +2g^{-+}_{1\perp}g^{-+}_{2\perp} - 2g^{+-}_{1\perp}g^{--}_{2\perp} \end{aligned} \tag{24}$$

$$\begin{aligned} \frac{\partial g^{+-}_{1\perp}}{\partial S} \;=\; & -2\left(2g^{+-}_{1\perp} - g^{--}_{2\perp}\right)g^{++}_{1\perp} + 2g^{+-}_{1\perp}g^{++}_{2\perp} \\ & -2g^{--}_{1\perp}g^{--}_{2\perp} - 2g^{+-}_{1\perp}g^{+-}_{2\perp} \end{aligned} \tag{25}$$

$$\frac{\partial g^{++}_{2\perp}}{\partial S} = -\left(g^{++}_{1\perp}\right)^2 - \left(g^{-+}_{1\perp}\right)^2 - \left(g^{-+}_{2\perp}\right)^2 + \left(g^{--}_{2\perp}\right)^2 \tag{26}$$

$$\frac{\partial g^{-+}_{2\perp}}{\partial S} = -2g^{++}_{1\perp}g^{-+}_{1\perp} - 2g^{++}_{2\perp}g^{-+}_{2\perp} + 2g^{-+}_{2\perp}g^{+-}_{2\perp} \tag{27}$$

$$\frac{\partial g^{--}_{2\perp}}{\partial S} = -2g^{--}_{1\perp}g^{+-}_{1\perp} + 2g^{++}_{2\perp}g^{--}_{2\perp} - 2g^{--}_{2\perp}g^{+-}_{2\perp} \tag{28}$$

$$\begin{aligned} \frac{\partial g^{+-}_{2\perp}}{\partial S} \;=\; & -\left(g^{--}_{1\perp}\right)^2 - \left(g^{+-}_{1\perp}\right)^2 \\ & +\left(g^{-+}_{2\perp}\right)^2 - \left(g^{--}_{2\perp}\right)^2 \end{aligned} \tag{29}$$

where $S = \ln l/(\pi v_F)$ is the RG time and l is the scaling quantity. We note that the couplings $g^{--}_{1\perp}$ and $g^{+-}_{2\perp}$ play important roles here. In general, those couplings are irrelevant when the hopping processes between two chains

are relevant[24,32,33,34,36]. However, there is no transverse hopping term in our model, so that we have to start from the picture of degenerate bands.

By solving the RG equations (22)-(29), we obtain the relations

$$g_{1\perp}^{+-}, g_{2\perp}^{--}, -g_{1\perp}^{--}, -g_{2\perp}^{+-} \gg g_{2\perp}^{++} \gg g_{1\perp}^{++} \gg 0 \qquad (30)$$

and $g_{-+}^{1\perp} = g_{2\perp}^{-+} = 0$ for $U \gtrsim J$. In this case, the parameters $K_{\rho-}$, $K_{\sigma+}$, and $K_{\sigma-}$ are scaled as $K_{\rho-} \to 0$, $K_{\sigma+} \to 0$, and $K_{\sigma-} \to \infty$. We therefore can simplify the second term of the phase Hamiltonian (14) as

$$\begin{aligned}&\left(g_{1\perp}^{+-} - g_{2\perp}^{--}\right)\cos 2\phi_{\rho-}\cos 2\phi_{\sigma-}\\ &+g_{1\perp}^{++}\cos 2\phi_{\sigma+}\cos 2\phi_{\sigma-} + g_{1\perp}^{+-}\cos 2\phi_{\rho-}\cos 2\phi_{\sigma+}\\ &+g_{1\perp}^{--}\cos 2\phi_{\sigma+}\cos 2\theta_{\sigma-} + g_{2\perp}^{--}\cos 2\phi_{\rho-}\cos 2\theta_{\sigma-}.\end{aligned} \qquad (31)$$

Note that the phase variables $\theta_{\rho-}$ and $\theta_{\sigma+}$ are not included in this term. Taking $g_{1\perp}^{++} > 0$ into account, we find that the fields $\phi_{\rho-}$ and $\phi_{\sigma+}$ are locked at $\langle\phi_{\rho-}\rangle = \frac{\pi}{2}I_1 + \pi I_2$ and $\langle\phi_{\sigma+}\rangle = \frac{\pi}{2}(I_1+1) + \pi I_3$ where I_n are integers.

Let us then turn to the $\sigma-$ mode that remains to be studied. The effective Hamiltonian of the $\sigma-$ mode takes the form

$$\begin{aligned}H_{\phi_{\sigma-}} &= \int dx \Big[K_{\sigma-}\left(\partial_x\theta_{\sigma-}\right)^2 + K_{\sigma-}^{-1}\left(\partial_x\phi_{\sigma-}\right)^2\\ &\quad +g_\phi\cos 2\phi_{\sigma-} + g_\theta\cos 2\theta_{\sigma-}\Big]\end{aligned} \qquad (32)$$

where $g_\phi = g_{1\perp}^{+-} - g_{2\perp}^{--} - g_{1\perp}^{++}$ and $g_\theta = g_{2\perp}^{--} - g_{1\perp}^{--}$. We here adopt a set of the variables $(\phi_{\rho-}, \phi_{\sigma+}) = (\pi I_1, \pi/2 + \pi I_2)$; however, it leads to a physically equivalent result if we chose another set $(\phi_{\rho-}, \phi_{\sigma+}) = (\pi/2 + \pi I_1, \pi I_2)$. For the Hamiltonian (32), there are three RG equations as follows:

$$\frac{dK_{\sigma-}}{dl} = y_\theta^2 - K_{\sigma-}^2 y_\sigma^2 \qquad (33)$$

$$\frac{dy_\phi}{dl} = \left(2 - 2K_{\sigma-}\right)y_\phi \qquad (34)$$

$$\frac{dy_\theta}{dl} = \left(2 - 2K_{\sigma-}^{-1}\right)y_\theta. \qquad (35)$$

where $y_\alpha = g_\alpha/(\pi v_F)$ with $\alpha = \theta, \phi$. Since $|y_\theta| \gg |y_\phi|$ and $K_{\sigma-} > 1$, the parameters are renormalized to $y_\theta \to \infty$, $y_\phi \to 0$, and $K_{\sigma-} \to \infty$. As a results, we find that three modes are locked as $\phi_{\rho-} = \frac{\pi}{2}I_1 + \pi I_2$, $\phi_{\sigma+} = \frac{\pi}{2}(I_1 + 1) + \pi I_3$, and $\theta_{\sigma-} = \frac{\pi}{2}(I_1+1) + \pi I_4$. Therefore, there is a gap in all the spin excitations.

C. Order parameters

In order to determine the dominant correlation, we introduce the order parameters of the superconducting correlations for four kinds of pairing symmetry, which are shown in Fig. 2. They are given in terms of the phase fields as follows:

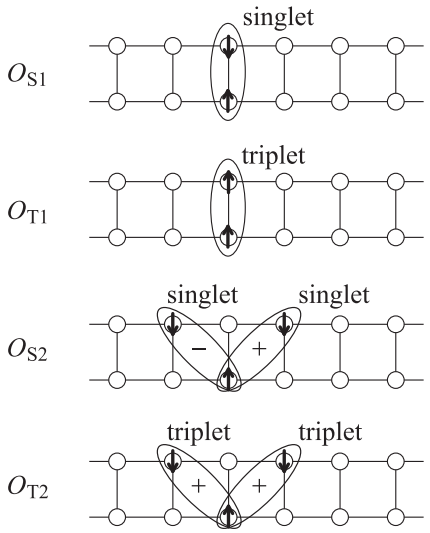

FIG. 2: Symmetry of the pairing state in the double-chain Hubbard model. The sign of the order parameter is also shown.

$$\begin{aligned}O_{S1} &= \sum_{p=\pm,\zeta=\pm}\psi_{p,\uparrow,\zeta}\psi_{-p,\downarrow,-\zeta}\\ &\sim \frac{2}{\pi a}e^{i\theta_{\rho+}}\left[\cos\theta_{\sigma-}\cos\phi_{\sigma+}\cos\phi_{\rho-}\right.\\ &\quad \left.-i\sin\theta_{\sigma-}\sin\phi_{\sigma+}\sin\phi_{\rho-}\right]\end{aligned} \qquad (36)$$

$$\begin{aligned}O_{T1} &= \sum_{p=\pm,\zeta=\pm}\zeta\psi_{p,\uparrow,\zeta}\psi_{-p,\downarrow,-\zeta}\\ &\sim \frac{2}{\pi a}e^{i\theta_{\rho+}}\left[i\sin\theta_{\sigma-}\cos\phi_{\sigma+}\cos\phi_{\rho-}\right.\\ &\quad \left.-\cos\theta_{\sigma-}\sin\phi_{\sigma+}\sin\phi_{\rho-}\right]\end{aligned} \qquad (37)$$

$$\begin{aligned}O_{S2} &= \sum_{p=\pm,\zeta=\pm}\zeta p\psi_{p,\uparrow,\zeta}\psi_{-p,\downarrow,-\zeta}\\ &\sim \frac{2i}{\pi a}e^{i\theta_{\rho+}}\left[i\sin\theta_{\sigma-}\sin\phi_{\sigma+}\cos\phi_{\rho-}\right.\\ &\quad \left.+\cos\theta_{\sigma-}\cos\phi_{\sigma+}\sin\phi_{\rho-}\right]\end{aligned} \qquad (38)$$

$$\begin{aligned}O_{T2} &= \sum_{p=\pm,\zeta=\pm}p\psi_{p,\uparrow,\zeta}\psi_{-p,\downarrow,-\zeta}\\ &\sim \frac{2i}{\pi a}e^{i\theta_{\rho+}}\left[\cos\theta_{\sigma-}\sin\phi_{\sigma+}\cos\phi_{\rho-}\right.\\ &\quad \left.+i\sin\theta_{\sigma-}\cos\phi_{\sigma+}\sin\phi_{\rho-}\right].\end{aligned} \qquad (39)$$

One can easily find that the inter-chain diagonal singlet pairing state, which corresponds to the order parameter O_{S2}, is only of the quasi-ordering superconducting instability when $\phi_{\rho-}$ and $\theta_{\sigma-}$ are locked. The asymptotic behavior of the S2 correlation function is given by

$$\left\langle O_{S2}^\dagger(r)O_{S2}(0)\right\rangle \sim \frac{1}{r^{1/2K_{\rho+}}}. \qquad (40)$$

and the other interchain pairing correlations decay exponentially. We also mention that all the intrachain pair-

ing correlations decay exponentially due to the locked modes. If we assume a S2 ground state $O^\dagger_{S2}|0\rangle$ and apply the interacting term of Hamiltonian (14) to the state, we obtain

$$H_I O^\dagger_{S2}|0\rangle = (g^{--}_{1\perp} - g^{+-}_{1\perp} - g^{--}_{2\perp} + g^{+-}_{2\perp})O^\dagger_{S2}|0\rangle\,. \quad (41)$$

Since $g^{--}_{1\perp} < 0$, $g^{+-}_{1\perp} > 0$, $g^{--}_{2\perp} > 0$, and $g^{+-}_{2\perp} < 0$, we find that the S2 pairing state can gain much energy.

The other possible order is the $4k_{\rm F}$ charge-density wave (CDW) correlation, of which the order parameter is given by

$$\begin{aligned} O_{4k_{\rm F}} &= \sum_{p,\sigma,\sigma'} \psi^\dagger_{p,\sigma,+}\psi^\dagger_{p,\sigma',-}\psi_{-p,\sigma',-}\psi_{-p,\sigma,+} \\ &\sim \frac{1}{a^2\pi^2}\cos\left(4k_{\rm F}x + 2\phi_{\rho+}\right)\left(\cos 2\phi_{\sigma+} + \cos 2\phi_{\sigma-}\right), \end{aligned} \quad (42)$$

where the $\cos 2\phi_{\sigma+}$ term comes from the cases where the spins are parallel $\sigma = \sigma'$, and the $\cos 2\phi_{\sigma-}$ term comes from the cases where the spins are antiparallel $\sigma = -\sigma'$. The latter component $\cos 2\phi_{\sigma-}$ decays exponentially because the field $\theta_{\sigma-}$ is locked. Thus, the $4k_{\rm F}$-CDW correlation shows a power-low behavior like

$$\left\langle O^\dagger_{4k_{\rm F}}(r) O_{4k_{\rm F}} \right\rangle \sim \frac{1}{r^{2K_{\rho+}}}. \quad (43)$$

By comparing Eq.(43) with Eq.(40), we find that the d_{xy}-wave-like S2 pairing correlation is most dominant for $K_{\rho+} > 0.5$, whereas the $4k_{\rm F}$-CDW is most dominant for $K_{\rho+} < 0.5$. This is the same as that of the standard two-band model.[33]

IV. NUMERICAL RESULTS

Next, we turn to the intermediate to strong coupling regime. We employ the Lanczos and DMRG methods to obtain energies and physical quantities in the ground state and low-lying excited states. In order to carry out our calculations, we consider N ($= N_\uparrow + N_\downarrow$) electrons in a system with length L (containing $2L$ sites). The electron density is given by $n = N/L$. Note that the number of electrons must be taken as $N = 4l$ with l (> 1) being an integer to maintain the total spin of the unpolarized ground state as $S = 0$.

For static quantities, we use the DMRG method with applying the open-end boundary conditions for precise calculations. We study systems with length up to $L = 128$ and keep up to $m \approx 2400$ density-matrix eigenstates in the DMRG procedure. In this way, the discarded weights are typically of the order $10^{-8} \sim 10^{-7}$ and the ground-state energy is obtained in the accuracy of $\sim 10^{-7}t$. All the calculated energies are extrapolated to the limit $m \to \infty$. For dynamical quantities, we use the Lanczos method for small clusters with the periodic boundary conditions. The system size is assumed as $L = 8$, i.e., 8×2 ladder.

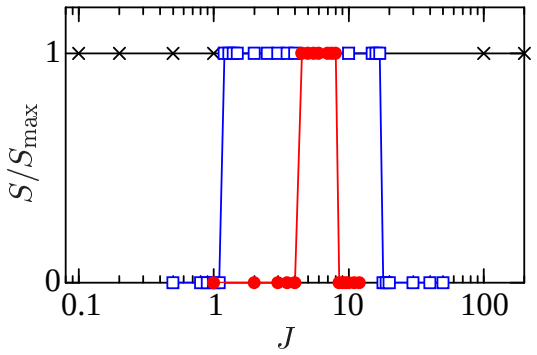

FIG. 3: (Color online) Calculated values of the total-spin quantum number S as a function of J for $U = 20$ (circles), 40 (squares), and ∞ (crosses). $L = 48$ and $n = 0.5$ are assumed.

A. Spin polarization

Approaching from the strong-coupling regime $U \gg t$, we may anticipate the presence of the fully-polarized ferromagnetic state. When the two chains are uncoupled, i.e., $J = 0$, the state can be interpreted as the Nagaoka state. Generally, the appearance of the Nagaoka state is limited to large-U and low-n range. However, the fully-polarized region would be spread into smaller-U and higher-n range if a finite J is introduced. This is because the polarized electrons can gain the kinetic energy without loss of the exchange interaction between the chains.

Let us start with investigating how the ferromagnetic phase appears in the parameter space (U, J). We can find it by calculating the expectation value of total-spin operator $\mathbf{S}$ in the ground state, which is defined by

$$\langle \mathbf{S}^2 \rangle = \sum_{ij} \langle \mathbf{S}_i \cdot \mathbf{S}_j \rangle = S(S+1). \quad (44)$$

For a fully-polarized state, one will obtain the total-spin quantum number $S = S_{\rm max} = N/2$, i.e., $S/S_{\rm max} = 1$. In Fig. 3, we show the total spin S normalized with respect to $S_{\rm max}$ as a function of J for several values of U. The system size and filling are fixed at $L = 48$ and $n = 0.5$, respectively. We calculate S for systems with length $L = 24$, 36, and 48, and confirm that the size dependence is negligible.

At $U = 20$, with increasing J, we find a transition from the paramagnetic state to the fully-polarized state at $J_{\rm c1} \sim 4.5$. Moreover, we find that the system goes back to the paramagnetic state at $J_{\rm c2} \sim 8.5$. This is because the formation of the local spin-singlet bound states gains more energy for very large values of J since J increases the gain in the spin-singlet binding energy as shown in Sec.IV B 3. We also find that the region with the full spin polarization broadens with increasing U. In the limit of $U = \infty$, $J_{\rm c1} \to 0$ and $J_{\rm c2} \to \infty$. We note that both of the transitions are discontinuous, i.e., of the first-order in the thermodynamic limit. Thus, the critical transition points can be determined in the parameter space (U, J),

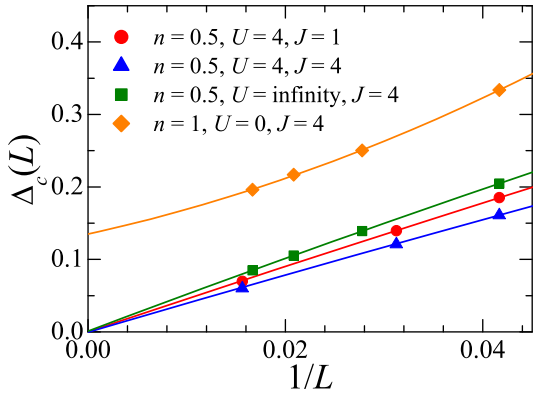

FIG. 4: (Color online) $\Delta_c(L)$ as a function of the inverse system length $1/L$. Lines are the fits with the 2nd-order polynomials.

which will be given as a ground-state phase diagram in Sec.IV F.

B. Excitation gaps

To ascertain the presence of the lowest excitation gap in the charge, spin, and pairing sectors, we calculate the charge gap, spin gap, and binding energy in the thermodynamic limit. We study several chains with lengths up to $L = 64$ and then perform the finite-size scaling analysis based on the size-dependence of each quantity.

1. *Charge gap*

The charge gap Δ_c is defined by

$$\Delta_c = \lim_{L\to\infty} \Delta_c(L), \tag{45}$$
$$\Delta_c(L) = E_L^0(N_\uparrow + 1, N_\downarrow + 1) + E_L^0(N_\uparrow - 1, N_\downarrow - 1) - 2E_L^0(N_e)$$

where $E_L^0(N_\uparrow, N_\downarrow)$ denotes the ground-state energy of a chain of length L with $N_\uparrow$ spin-up and $N_\downarrow$ spin-down electrons. In Fig. 4, we plot the charge gap $\Delta_c(L)$ as a function of the inverse system length $1/L$ for several parameter sets.

At half filling ($n = 1$), we can easily expect the system to be a Mott insulator for $U > 0$. However, we also find the system is insulating even for $U = 0$ if J is finite. This is associated with the fact that a localized spin-triplet pair is formed on each rung. If an electron is add to the rung, an effective on-rung repulsive interaction $U_{\rm eff} = U + \frac{J}{2}$ acts. Thus, we obtain the effective Hamiltonian near half filling

$$H_{\rm eff}^{n\sim 1} = -t\sum_{r_x,\sigma}(c^\dagger_{r_x,\sigma}c_{r_x,\sigma} + \text{H.}c.) + \left(U + \frac{J}{2}\right)\sum_{r_x,\sigma} n^T_{r_x} n_{r_x,\sigma}\delta_{\langle S^z_{r_x}\rangle,\pm\frac{1}{2}} \tag{46}$$

where $c_{r_x,\sigma} = c_{r_x,1,\sigma}c_{r_x,2,\sigma}$ is the annihilation operator of an electron with spin σ at rung r_x, $n_{r_x,\sigma} = c^\dagger_{r_x,\sigma}c_{r_x,\sigma}$ is the number operator, $S^z_{r_x} = n_{r_x,\uparrow} - n_{r_x,\downarrow}$ is the z-component of total spin, and $n^T_{r_x} = T^\dagger_{r_x}T_{r_x}$ with the spin-triplet operator $T_{r_x} = c_{r_x,1,\sigma}c_{r_x,2,\sigma}$ or $\frac{1}{\sqrt{2}}(c_{r_x,1,\sigma}c_{r_x,2,\bar\sigma} + c_{r_x,1,\bar\sigma}c_{r_x,2,\sigma}$.

Let us then turn to the case away from half filling. There are two points to be noted here: one is whether the system is insulating at quarter filling ($n = 0.5$) as is the case of the Hubbard and $t-J$ ladder; the other is whether the phase separation occurs in the fully-polarized state. As seen in Fig. 4, all the results for $n = 0.5$ are smoothly extrapolated to zero in the thermodynamic limit $1/L \to 0$. At $U = \infty$ and $J = 4$, the system is in the fully-polarized state. We therefore conclude that the system is metallic in the entire region except $n = 1$.

2. *Spin gap*

The spin gap Δ_s is defined by

$$\Delta_s = \lim_{L\to\infty} \Delta_s(L), \tag{47}$$
$$\Delta_s(L) = E_L^0(N_\uparrow + 1, N_\downarrow - 1) - E_L^0(N_\uparrow, N_\downarrow).$$

In Fig. 5, we plot the spin gap $\Delta_s(L)$ as a function of inverse system length $1/L$ at (a) $n = 1$ and (b) $n = 0.75$. For $U = 4, n = 1$ and $U = 1, n = 0.75$, values of $\Delta_s(L)$ seem to be smoothly extrapolated to zero when $1/L \to 0$, which is in contrast to the weak-coupling analysis. For the other cases, however, the extrapolated lines reach zero at finite values of $1/L$. This is unphysical and so it may be a good guess that $\Delta_s(L)$ is fairly flat around $1/L = 0$, as seen in the results for $U = 4, n = 1$ and $U = 1, n = 0.75$. Unfortunately, we cannot treat the large enough systems to confirm if this is the case. Nevertheless, if we assume that the $1/L$-dependence of $\Delta_s(L)$ reflects the spinon band structure near the Fermi point, the flat behavior of $\Delta_s(L)$ may rather imply the presence of a spin gapful state. Since we cannot detect the spin gap less than $\sim 10^{-6}$ within the present calculations, the existence of a very small spin gap, i.e., $\Delta(L \to \infty) \lesssim 10^{-6}$, is conceivable.

To determine if the spin gap is present or absent, we also calculate the equal-time spin-spin correlation function

$$S(|r_x - r'_x|, r_y, r'_y) = \langle S^z_{r_x,r_y} S^z_{r'_x,r'_y}\rangle - \langle S^z_{r_x,r_y}\rangle\langle S^z_{r'_x,r'_y}\rangle, \tag{48}$$

where $S^z_{r_x,r_y}$ is the z component of the spin operator of an electron at site r_x on rung r_y. In Fig. 5, we present

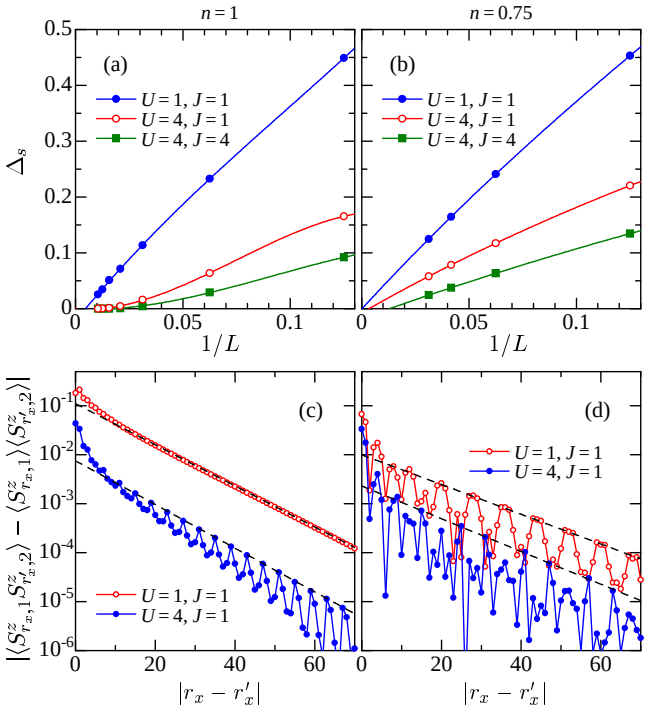

FIG. 5: (Color online) Upper panels: $\Delta_s(L)$ as a function of inverse system size for (a) $n = 1$ and (b) $n = 0.75$. Solid lines are the polynomial fits to the data for the finite-size scaling analysis. Lower panels: Semilogarithmic plot of the magnitude of the spin-spin correlation function $S(|r_x - r'_x|, 1, 2')$ at $J = 1$ for (c) $n = 1$ and (d) $n = 0.75$. The data are fitted with a function $S(|r_x - r'_x|, 1, 2) \simeq \exp\left(-\frac{|r_x - r'_x|}{\xi}\right)$.

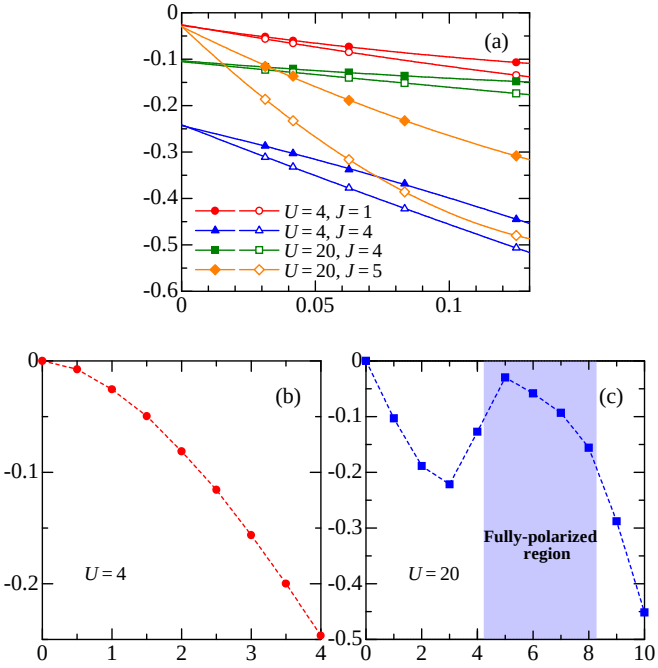

FIG. 6: (Color online) Upper panel: $\Delta_B^{\pm}(L)$ as a function of inverse system length $1/L$ at $n = 0.5$. Solid lines are the polynomial fits to the data for finite-size scaling analysis. Solid (empty) symbols denote the binding energy of electrons (holes). Lower panels: Values of $\Delta_B^{\pm}(L)$ extrapolated to $1/L \to 0$ plotted as a function of J for (b) $U = 4$ abd (c) $U = 10$.

a semilogarithmic plot of $|S(|r_x - r'_x|, 1, 2)|$ as a function of the distance $|r_x - r'_x|$ for (c) $n = 1$ and (d) $n = 0.75$. Note that the long-range behavior of $|S(|r_x - r'_x|, 1, 1)|$ is almost the same as that of $|S(|r_x - r'_x|, 1, 2)|$. The results can be fitted with a function $\exp(-|r_x - r'_x|/\xi)$ and thus the exponential decay of the correlation functions is confirmed for all the parameter sets. The correlation lengths are estimated as $\xi = 10.35(9.74)$ for $U = 1(4)$ at $n = 1$; $\xi = 14.29(12.99)$ for $U = 1(4)$ at $n = 0.75$. According to the Tomonaga-Luttinger liquid theory, the spin-spin correlation can decay exponentially only when there is a gap in all the magnetic excitations. Consequently, it would be rather appropriate to conclude that there exists quite small spin gap ($\lesssim 10^{-6}$). The correlation lengths seem to be much longer than those of other standard spin-gapped systems, e.g.,$\xi = 3.19$ in the two-leg isotropic Heisenberg system. However, it has been found that in the zigzag Heisenberg chain, the correlation lengths increase rapidly with decreasing binding energy.[38] Thus, the very large values of ξ may reflect an exponentially small spin gap.

3. *Binding energy*

The binding energy $\Delta_B^{\pm}$ is defined by

$$\Delta_B^{\pm} = \lim_{L\to\infty} \Delta_B^{\pm}(L), \tag{49}$$
$$\Delta_B^{\pm}(L) = E_L^0(N_\uparrow \pm 1, N_\downarrow \pm 1) + E_L^0(N_\uparrow, N_\downarrow) - 2E_L^0(N_\uparrow \pm 1, N_\downarrow)$$

where the + (−) sign corresponds to the binding energy of electrons (holes). In Fig. 6 (a), we plot the binding energy $\Delta_B^{\pm}(L)$ as a function of the inverse system length $1/L$ at $n = 0.5$ for several sets of parameters. For all the parameter sets, $|\Delta_B^{\pm}(L)|$ is found to decrease monotonically as a function of $1/L$, so that we can extrapolate $|\Delta_B^{\pm}(L)|$ to the thermodynamic limit systematically. We perform a least-squares fit of $|\Delta_B^{\pm}(L)|$ to a polynomial in $1/L$ and obtain the extrapolated values. We note that the binding energies of electrons and holes are extrapolated to the same value at $1/L \to 0$.

In Fig. 6 (b), the extrapolated values of $\Delta_B^{\pm}$ for $U = 4$ as a function of J are shown. When U is small, the system is expected to be in the spin-singlet superconducting phase, as discussed in Sec. III. Hence, the binding energy is determined by an energy of the spin-singlet bound state. In analogy with the Haldane gap, we expect a scaling $\Delta_B^{\pm} \propto Jt/U^2$ from perturbation assuming the double

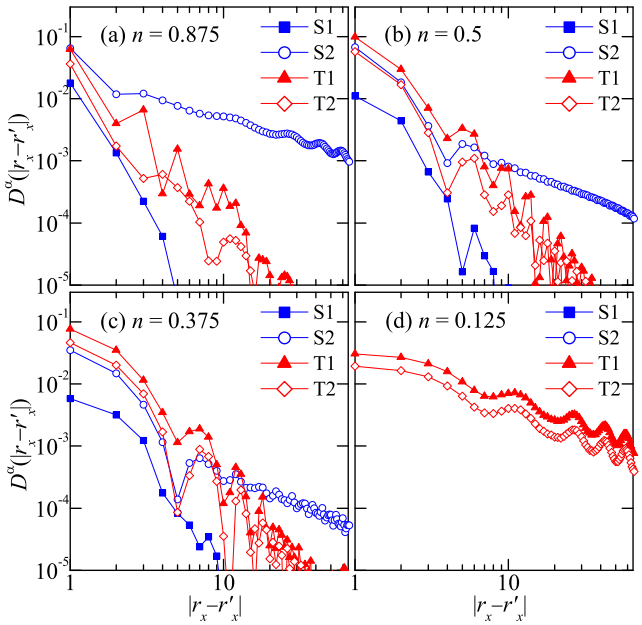

FIG. 7: (Color online) Log-log plot of the pair-correlation functions $D^{\alpha}(|r_x - r'_x|)$ calculated for $L = 128$ at (a) $n = 0.825$, $U = 10$, $J = 2$, (b) $n = 0.5$, $U = 10$, $J = 4$, and (c) $n = 0.25$, $U = 10$, $J = 5$.

occupancy is sufficiently excluded. The origin of this energy gain is also interpreted as the double exchange interaction in our model. For small J, this estimation seems not to work well. However, the double occupancy is increasingly excluded with increasing J and thus $|\Delta_B^{\pm}(L)|$ increases linearly with J at $J \gtrsim 3$. In Fig. 6 (c), the extrapolated values of $\Delta_B^{\pm}$ for $U = 20$ as a function of J are shown. Since the double occupancy is almost excluded, $|\Delta_B^{\pm}|$ increases linearly with J even if J is small. It is notable that the binding energy is strongly suppressed in the fully-polarized phase. This phase is regarded as the spin-triplet superconducting one, where the binding energy is determined by an energy of the spin-triplet bound state, which is scaled as $|\Delta_B^{\pm}| \propto J - J_{c1}$. Generally, an energy of the spin-triplet bound state is much lower than that of the spin-singlet bound state.[39]

C. Superconducting correlation

For our model, we can consider four kinds of superconducting correlations as mentioned in Sec.III. In order to estimate them numerically, we define the corresponding pair correlation functions as

$$D^{\alpha}(|r_x - r'_x|) = \left\langle \Delta_{\alpha}^{\dagger}(r_x)\Delta_{\alpha}(r'_x) \right\rangle \tag{50}$$

with

$$\Delta_{S1}(r_x) = c_{r_x,1,\uparrow}c_{r_x,2,\downarrow} - c_{r_x,1,\downarrow}c_{r_x,2,\uparrow} \tag{51}$$
$$\Delta_{T1}(r_x) = c_{r_x,1,\uparrow}c_{r_x,2,\downarrow} + c_{r_x,1,\downarrow}c_{r_x,2,\uparrow} \tag{52}$$
$$\Delta_{S2}(r_x) = c_{r_x,1,\uparrow}c_{r_x+1,2,\downarrow} - c_{r_x,1,\downarrow}c_{r_x+1,2,\uparrow} \tag{53}$$
$$\Delta_{T2}(r_x) = c_{r_x,1,\uparrow}c_{r_x+1,2,\downarrow} + c_{r_x,1,\downarrow}c_{r_x+1,2,\uparrow}, \tag{54}$$

which are calculated by the DMRG method. The calculated results for three sets of parameters are shown in Fig. 7. For $n = 0.825$, $U = 10$, and $J = 4$ [Fig. 7(a)], the S2 pairing correlation is clearly the most dominant one, which shows a power-law length dependence. The ratio of the decay is estimated to be $\sim r^{-0.7}$, which leads to $K_{\rho}^{+} = 0.714$. This is consistent with the bosonization result for the spin gapful state. At $n = 0.5$, $U = 10$, $J = 4$ [Fig. 7(b)], the system has a $S = 0$ ground state but is somewhat closer to the fully-polarized ferromagnetic phase. The S2 pairing correlation is still the most dominant one but the T1 pairing correlation becomes much enhanced at a short distance $|r_x - r'_x| \lesssim 10$. This is because the formation of a local spin-triplet bound state on a rung can gain some energies. We note that the T2 pairing correlation is also enhanced, reflecting a tendency to the fully-polarized ferromagnetic state. The decay ratio of the S2 correlation is $\sim r^{-0.8}$, which leads to $K_{\rho}^{+} = 0.625$. This value agrees well with our direct estimation of K_{ρ}^{+} (See Sec.IV E). If the system further approaches the fully-polarized ferromagnetic phase [Fig. 7(c)], the change in the correlation functions at short ranges becomes more prominent. Surprisingly, we find that the decay lengths of all the correlations are almost unchanged as far as J is fixed in the $S = 0$ ground state. In the fully-polarized ferromagnetic phase [Fig. 7(d)], the T1 pairing correlation is the most dominant one and only the S2 pairing correlation is competing. The decay ratio of both correlation functions is $\sim r^{-1}$, which leads to $K_{\rho}^{+} = 0.5$.

D. Anomalous Green function

Let us now determine the pairing symmetry in the S2 superconducting state. To this end, we calculate the one-particle anomalous Green function,[40] which exhibits the excitations of the Bogoliubov quasiparticles in the BCS theory. Therefore, we can see how the nodes appear in the superconducting gap function. The anomalous Green function is defined by

$$G_{k_y,k'_y}(q_x, z) = \left\langle \psi_0^{N_e-2} \right| c_{q_x,k_y,\uparrow} \frac{1}{z - H + E_0} c_{-q_x,k'_y,\downarrow} \left| \psi_0^{N_e} \right\rangle \tag{55}$$

where $\left|\psi_0^{N_e}\right\rangle$ denote the wavefunction of the ground state with $N_e/2$ up-spin and $N_e/2$ down-spin electrons, and E_0

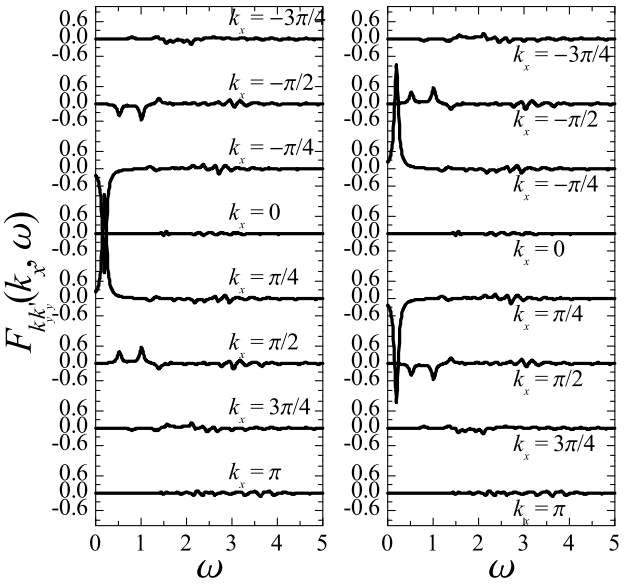

FIG. 8: Left panel: Anomalous Green's function at $k_y = 0$, $k'_y = \pi$, $n = N_e/N = 5/8$, $U = 10$, $J = 2$, and $N = 16$. Right panel: Same as the left panel but at $k_y = \pi$, $k'_y = 0$.

is chosen as the average value of $E_L^0(N_\uparrow - 1, N_\downarrow - 1)$ and $E_L^0(N_\uparrow, N_\downarrow)$. We then estimate the spectral function as

$$F_{k_y,k'_y}(k_x) = -\frac{1}{\pi}\mathrm{Im}G_{k_y,k'_y}(q_x, \omega + i\eta) \tag{56}$$

with $\eta = 0^+$ and its frequency integral as

$$F_{k_y,k'_y}(k_x) = \left\langle \psi_0^{N_e-2} \middle| c_{k_x,k_y,\uparrow} c_{-k_x,k'_y,\downarrow} \middle| \psi_0^{N_e} \right\rangle . \tag{57}$$

We calculate the anomalous Green function (55) for the ladder with length $L = 8$ by using the Lanczos method. We should note that the BCS theory is not readily applicable for (quasi) one-dimensional system; actually, $F_{k_y,k'_y}(q_x)$ is not long-range ordered with a logarithmic decay as a function of L. However, apart from this prefactor, we can naively expect that $F_{k_y,k'_y}(q_x)$ calculated on finite-size systems should provide information on the pairing symmetry at intermediate distances.

The calculated results for $F_{k_y,k'_y}(k_x,\omega)$ are shown in Fig. 8. We can observe pronounced low-energy peaks at $|k_x| = \frac{\pi}{4}$ for all k_y and k'_y, which are the nearest to the Fermi momenta $k_\mathrm{F}(= \frac{5}{16}\pi)$, and much smaller peaks at higher energies for other momenta. We also find that the spectral weight vanishes at $q_x = 0$, $q_x = \pi$, and $k_y = k'_y$. The weights of the peaks appear to be similar to the BCS form of the condensation amplitude, which has a maximum value at the Fermi momenta. We may thus assume that the superconducting ground state in strongly correlated electron systems can be characterized by a gap function, which is directly proportional to the frequency-integrated function $F_{k_y,k'_y}(q_x)$.[40,41] The function $F_{k_y,k'_y}(k_x)$ obeys the relation $F_{k_y,k'_y}(k_x) = -F_{k'_y,k_y}(k_x)$ and $F_{k_y,k'_y}(k_x) = -F_{k_y,k'_y}(-k_x)$. This indicates the formation of the d_{xy}-wave like pairing state in our system, which is consistent with the weak-coupling results shown in Sec.III C.

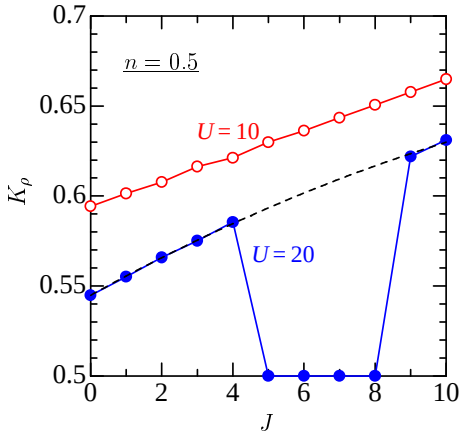

FIG. 9: (Color online) DMRG results for $K_{\rho+}$ as a function of J. The results for $U = 10$ and 20 at $n = 0.5$ are shown. Dotted line is guide for eyes.

E. Tomonaga-Luttinger liquid parameter

For the calculation of the TL parameter, we use a recently proposed method of the DMRG technique.[42] As mentioned in Sec. III C, the TL parameter K_ρ^+ determines the long-range decays of the d_{xy}-like (S2) pairing and $4k_F$-CDW correlations in the metallic TL-liquid ground state, whereas the parameter K_ρ^- is scaled as $K_\rho^- \to 0$. For the double-chain model, we define the TL parameter as

$$K_{\rho\pm} = \frac{\pi}{2}\lim_{q\to 0}\frac{\partial N_\pm(q)}{\partial q} \tag{58}$$

with

$$N_\pm(q) = \frac{1}{L}\sum_{r_x,r'_x} e^{iq(r_x - r'_x)} \left\langle n_{r_x}^\pm n_{r'_x}^\pm \right\rangle . \tag{59}$$

where $n_{r_x}^\pm = n_{r_x,1} \pm n_{r_x,2}$. In Fig. 9, we show the calculated results for $K_{\rho+}$ as a function of J for $U = 10$ and 20 at $n = 0.5$. For $U = 10$, K_ρ^+ increases monotonously with increasing J, which is consistent with the monotonous increase in the binding energy with respect to J in the strong-coupling regime. For $U = 20$, the behaviors for $J \lesssim 4$ and $J \gtrsim 9$ are quite similar to those for $U = 10$, although the values are somewhat smaller due to the effects of the Umklapp scattering. However, we estimate the TL parameter as $K_\rho^+ = 0.5$ for $5 \lesssim J \lesssim 8$. This regime corresponds to the fully-polarized ferromagnetic phase and the TL parameter should be the same as that of a spinless fermion system. We thus find $K_\rho > 1/2$ in

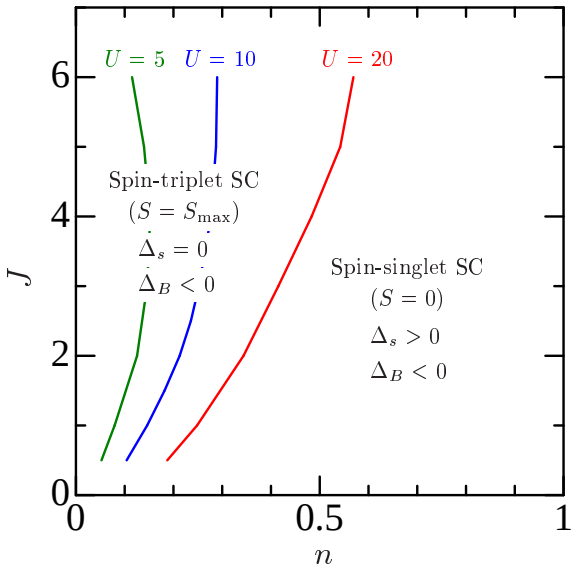

FIG. 10: (Color online) Phase diagram of our double-chain Hubbard model obtained from the DRMG calculations. The phase boundary between the fully-polarized ferromagnetic phase and d_{xy}-like superconducting (SC) phase is shown for $U = 5$, 10, and 20.

the entire region except in the fully-polarized ferromagnetic phase and we confirm that the S2-type superconducting correlation is most dominant.

F. Phase diagram

In Fig. 10, we show the phase diagram of our model in the parameter space (n, J) for $U = 5$, 10, and 20. The phase boundary is determined by the calculated results for the total-spin quantum number. At higher electron concentrations from the phase boundary, the system is characterized as the S2-type spin-singlet superconducting state, and at lower concentrations from the phase boundary, the system is characterized as the fully-polarized ferromagnetic state and simultaneously as the T1-type spin-triplet superconducting state. We note that the fully-polarized ferromagnetic phase is spread to the higher concentration range with increasing U, and it occupies the entire parameter region $(n < 1, J > 0)$ at $U = \infty$. This result is connected to the Nagaoka state[4] at $U \to \infty$.

V. SUMMARY AND DISCUSSION

We have studied the ground-state properties of the double-chain Hubbard model coupled with ferromagnetic exchange interaction by using the weak-coupling theory, DMRG technique, and the Lanczos method. We have thereby determined the ground-state phase diagram in the parameter space of the ferromagnetic exchange interaction and band filling. We have found that, in high electron density regime, the spin gap opens and the spin-singlet d_{xy}-wave-like pairing correlation is most dominant, and in low electron density regime, the fully-polarized ferromagnetic state is stabilized and simultaneously the spin-triplet p_y-wave-like pairing correlation becomes most dominant.

Here, let us make some comment on what happens if some additional terms are introduced to our model. First, we consider the case where the hopping integral between the two chains $t_\perp$ is added. In this case, the couplings $g_{1\perp}^{--}$ and $g_{2\perp}^{+-}$ become irrelevant, which leads to a collapse of the pairing state between different bands, i.e., $k_y = 0$ and π. Thus, the spin-singlet superconductivity is suppressed. Since the term $t_\perp$ induces the antiferromagnetic interaction on each rung, the spin-triplet superconductivity may also be suppressed. Next, we consider the case where the intersite Coulomb interaction between the two chains $V_\perp$ is added. In this case, we can easily imagine that the spin-triplet superconductivity is strongly suppressed because the d_y-wave-like pairing state is formed on rung. The double exchange interaction for the d_{xy}-wave-like pairing state is also suppressed.

Finally, let us discuss possible relationship between the present model and the model of two Hubbard chains coupled with zigzag bonds where the spin-triplet superconductivity has been shown to occur.[17,18,19] The two models in the strong-coupling regime have the following features in common: (i) the superconductivity occurs near the region of ferromagnetism, (ii) there is a competition between the spin-singlet and spin-triplet pairings, and (iii) the spin-gap is quite small or vanishes. These situations may well suggest that the spin-triplet pairing could be dominant in the present model near the phase boundary between the spin-singlet superconductivity and ferromagnetism. So far, we have not found any indications that the spin-triplet pairing becomes more dominant than the spin-singlet pairing unless the ground state is spin polarized. We hope that this point will be clarified with more elaborate calculations done in future.

Acknowledgments

We thank S. Ejima, H. Matsueda, K. Sano, and H. Yoshioka for useful discussions. This work was supported in part by Grants-in-Aid for Scientific Research (Nos. 18028008, 18043006, 18540338, and 19014004) from the Ministry of Education, Science, Sports and Culture of Japan. A part of computations was carried out at the Research Center for Computational Science, Okazaki Research Facilities, and the Institute for Solid State Physics, University of Tokyo.

[1] J. Hubbard, Proc. Roy. Soc. (London) A **276**, 238 (1963).
[2] J. Kanamori, Prog. Theor. Phys. **30**, 275 (1963).
[3] A. Mielke and H. Tasaki, Comm. Math. Phys. **158**, 341 (1993); H. Tasaki, Comm. Math. Phys. **242**, 445 (2003).
[4] Y. Nagaoka, Phys. Rev. **147**, 392 (1966).
[5] D. J. Thouless, Proc. Phys. Soc. Lond. **86**, 893 (1965).
[6] A. Mielke, J. Phys. **A24**, L73 (1991).
[7] H. Tasaki, Phys. Rev. Lett. **69**, 1608 (1992).
[8] C. Zener, Phys. Rev. **81**, 440 (1951); **82**, 403 (1951).
[9] J. H. Van Vleck, Rev. Mod. Phys. **25**, 220 (1953).
[10] J. C. Slater, H. Statz, and G. F. Koster, Phys. Rev. **91**, 1323 (1953).
[11] K. Penc, H. Shiba, F. Mila, and T. Tsukagoshi, Phys. Rev. B **54**, 4056 (1996).
[12] P. Fazekas, *Lecture Notes on Electron Correlation and Magnetism* (World Scientific, Singapore, 1999), p. 435.
[13] S. S. Saxena, P. Agarwal, K. Ahilan, F. M. Grosche, R. K. W. Haselwimmer, M. J. Steiner, E. Pugh, I. R. Walker, S. R. Julian, P. Monthoux, G. G. Lonzarich, A. Huxley, I. Sheikin, D. Braithwaite, and J. Flouquet, Nature **406**, 587 (2000).
[14] D. Aoki, A. Huxley, E. Ressouche, D. Braithwaite, J. Flouquet, J-P. Brison, E. Lhotel, and C. Paulsen, Nature **413**, 613 (2001).
[15] C. Pfleiderer, M. Uhlarz, S. M. Hayden, R. Vollmer, H. von Loehneysen, N. R. Bernhoeft, and G. G. Lonzarich, Nature **412**, 58 (2001).
[16] D. Fay and J. Appel, Phys. Rev. B **22**, 3173 (1980).
[17] Y. Ohta, S. Nishimoto, T. Shirakawa, and Y. Yamaguchi, Phys. Rev. B **72**, 012503 (2005).
[18] S. Nishimoto, T. Shirakawa, and Y. Ohta, Phys. Rev. B **77**, 115102 (2008).
[19] S. Nishimoto, K. Sano, and Y. Ohta, Phys. Rev. B **77**, 085119 (2008).
[20] J. Sólyom, Adv. Phys. **28**, 201 (1979).
[21] S. R. White, Phys. Rev. Lett. **69**, 2863 (1992); Phys. Rev. B **48**, 10345 (1993).
[22] C. Lanczos, *Applied Analysis* (Prentice-Hall, Englewood Cliffs, NJ, 1956).
[23] S. Fujimoto and N. Kawakami, Phys. Rev. B **52**, 6189 (1995).
[24] D. V. Khveshchenko and T. M. Rice, Phys. Rev. B **50**, 252 (1994).
[25] D. G. Shelton and A. M. Tsvelik, Phys. Rev. B **53**, 14036 (1996).
[26] B. Ammon and M. Imada, J. Phys. Soc. Japan **70**, 547 (2000).
[27] H. Sakamoto, T. Momoi, and K. Kubo, Phys. Rev. B **65** 224403 (2002).
[28] N. Nagaosa and M. Oshikawa: J. Phys. Soc. Jpn. **65**, 2241 (1996).
[29] V. J. Emery, in *Highly Conducting One-Dimensional Solids*, edited by J. T. Devreese *et al.* (Plenum, New York, 1979); H. Fukuyama and H. Takayama, in *Electronic Properties of Inorganic Quasi-One-Dimensional Materials*, edited by P. Monceau (Reidel, Dordrecht, 1985).
[30] C. M. Varma and A. Zawadowski, Phys. Rev. B **32** 7399 (1985).
[31] A. A. Nersesyan, Phys. Lett. A **153**, 49 (1991); A. A. Nersesyan, A. Luther, and F. Kusmartsev, Phys. Lett. A **176**, 363 (1993).
[32] M. Fabrizio, Phys. Rev. B **48**, 15838 (1993).
[33] H. J. Schulz, Phys. Rev. B **53**, R2959 (1996).
[34] L. Balents and M. P. A. Fisher, Phys. Rev. B **53**, 12133 (1996).
[35] E. Orignac and T. Giamarchi, Phys. Rev. B **56**, 7167 (1997).
[36] M. Tsuchiizu, P. Donohue, Y. Suzumura, and T. Giamarchi, Eur. Phys. J. B **19**, 185 (2001); P. Donohue, M. Tsuchiizu, T. Giamarchi, and Y. Suzumura, Phys. Rev. B **63**, 045121 (2001).
[37] J. O. Fjærestad and J. B. Marston, Phys. Rev. B **65**, 125106 (2002).
[38] S. R. White and I. Affleck, Phys. Rev. B **54**, 9862 (1996).
[39] Phys. Rev. **147**, 223 (1966).
[40] Y. Ohta, T. Shimozato, R. Eder, and S. Maekawa, Phys. Rev. Lett. **73**, 324 (1994).
[41] D. Poilblanc, D. J. Scalapino, and S. Capponi, Phys. Rev. Lett. **91**, 137203 (2003).
[42] S. Ejima, F. Gebhard, and S. Nishimoto, Europhys. Lett. **70**, 492 (2005).